

Published in final edited form as:

Nat Cell Biol. 2017 April ; 19(4): 391–398. doi:10.1038/ncb3481.

Tubulin acetylation protects long-lived microtubules against mechanical aging

Didier Portran¹, Laura Schaedel², Zhenjie Xu¹, Manuel Théry^{2,3}, and Maxence V. Nachury^{1,*}

¹Department of Molecular and Cellular Physiology, Stanford University School of Medicine, CA 94305, USA

²Laboratoire de Physiologie Cellulaire et Végétale, Institut de Recherche en Technologie et Science pour le Vivant, UMR5168, CEA/INRA/CNRS/UGA, 38054 Grenoble, France

³Unité de Thérapie Cellulaire, Hôpital Saint Louis, Institut Universitaire d'Hématologie, UMRS1160, INSERM/AP-HP/Université Paris Diderot, 75010 Paris, France

Introductory Paragraph

Long-lived microtubules endow the eukaryotic cell with long-range transport abilities. While long-lived microtubules are acetylated on lysine 40 of α -tubulin (α K40), acetylation takes place after stabilization¹ and does not protect against depolymerization². Instead, α K40 acetylation has been proposed to mechanically stabilize microtubules³. Yet how modification of α K40, a residue exposed to the microtubule lumen and inaccessible from MAPs and motors^{1,4}, could affect microtubule mechanics remains an open question. Here we develop FRET-based assays that report on the lateral interactions between protofilaments and find that α K40 acetylation directly weakens inter-protofilament interactions. Congruently, α K40 acetylation affects two processes largely governed by inter-protofilament interactions, reducing the nucleation frequency and accelerating the shrinkage rate. Most relevant to the biological function of acetylation, microfluidics manipulations demonstrate that α K40 acetylation enhances flexibility and confers resilience against repeated mechanical stresses. Thus, unlike deacetylated microtubules that accumulate damages when subjected to repeated stresses, long-lived microtubules are protected from mechanical aging through their acquisition of α K40 acetylation. Thus, unlike other tubulin post-translational modifications that act through MAPs, motors and severing enzymes, intraluminal acetylation directly tunes the compliance and resilience of microtubules.

Users may view, print, copy, and download text and data-mine the content in such documents, for the purposes of academic research, subject always to the full Conditions of use:http://www.nature.com/authors/editorial_policies/license.html#terms

*Correspondence and requests for materials should be addressed to M.V.N. (nachury@gmail.com).

Author Contributions

Z.X. was involved in the initial conceptualization of the project. M.V.N. and M.T. designed the study. D.P. developed and conducted the enzymatic modifications of tubulin, self-assembly assays and electron microscopy. L.S. performed the measurement and analysis of microtubule persistence length and material fatigue. M.V.N. and D.P. wrote the manuscript with input from all authors.

Author Information

The authors declare no competing financial interests.

Keywords

Microtubule; α TAT1; α K40 acetylation; persistence length; flexibility; protofilaments lateral interaction

Microtubules with hour-long half-lives found in cytoplasm, cilia and axons must preserve their structural integrity in the face of ubiquitous mechanical stresses to maintain tracks for intracellular transport. Paradoxically, while microtubules assembled *in vitro* have millimeter-long persistence lengths and are as stiff as Plexiglas^{5,6}, long-lived microtubules in cells are frequently highly buckled due to the compressive loads generated by microtubule-based molecular motors and actomyosin contractility^{7,8}. How long-lived microtubules acquire mechanical stability is not known.

α K40 acetylation has recently emerged as a candidate for the mechanical stabilization of microtubules because nematodes mutant for the α K40 acetyltransferase α TAT1/MEC-17 experience profound microtubule defects including protofilament number variability, fragmentation and lattice opening^{9–11}. To characterize the biochemical consequences of α K40 acetylation, we enzymatically modified brain tubulin (30% acetylated) then removed the enzymes to generate pure preparations of acetylated (>96%) and deacetylated (<1% acetylated) tubulin (Fig. 1a and Supplementary Fig. 1a,b,c). Absolute levels of acetylation were determined by comparison with ciliary tubulin, a standard known to be 100% acetylated¹². Surprisingly, acetylated tubulin self-assembled much slower than deacetylated tubulin while brain tubulin showed intermediate kinetics (Fig. 1b). The effects of TAT1 and SIRT2 on microtubule self-assembly were fully reversible (Supplementary Fig. 1d-f), confirming that it is acetylation *per se* and not the enzymes themselves that impinge on the kinetics of polymerization. Self-assembly of tubulin is kinetically limited by nucleation and reaches an apparent steady-state once polymerization and depolymerization balance one another. Consistent with the increased lag phase of self-assembly for acetylated tubulin, acetylation decreased the spontaneous nucleation rate by 2.7-fold (Fig. 1c, Supplementary Fig. 2a,b). Further supporting the conclusion that acetylation reduces microtubule nucleation, addition of pre-formed microtubule seeds to acetylated tubulin rapidly accelerated self-assembly and the steady-state levels of microtubules became nearly identical between deacetylated and acetylated samples once seeds had been supplied (Fig. 1d). The pronounced effects of acetylation on nucleation of pure tubulin demonstrate that acetylation directly regulates a molecular interaction within the microtubule lattice without the need for a molecular intermediate. We thus sought to pinpoint the specific molecular interactions within the lattice that are altered by acetylation.

Microtubule nucleation is thought to entail the assembly of short protofilaments through longitudinal (i.e. head-to-tail) interactions between α/β -tubulin dimers, the formation of small sheets through parallel inter-protofilament interactions; lateral and longitudinal extension then lead to sheet closure into a 13- to 15-protofilament tube¹³ (Fig. 1e). Similarly, microtubule polymerization and depolymerization are governed by longitudinal and lateral interactions but in subtly different ways. Microtubule depolymerization entails the outward curving of protofilaments imparted by the GDP-bound conformation of tubulin

and peeling of protofilaments away from one other¹⁴. The relative energetics of outward protofilament bending and lateral cohesion between neighboring protofilaments is thus expected to govern depolymerization¹⁵. Meanwhile, in the elongating microtubule, a GTP cap is predicted to lock protofilaments into a straight conformation and the rate of subunit addition is most closely influenced by longitudinal interactions (see model in Fig. 1e). Consequently, the strengthening of lateral interprotofilament interactions is expected to slow depolymerization while minimally affecting growth rates¹⁶. Measurements of single microtubule dynamics showed no detectable difference in the growth rate of deacetylated and acetylated microtubules (Fig. 1f and Supplementary Fig. 2b). Strikingly, acetylated microtubules depolymerized threefold faster than deacetylated microtubules (Fig. 1f and Supplementary Fig. 2b). These data are consistent with lateral, but not longitudinal, interactions being reduced by acetylation.

To more directly assess the dynamics of longitudinal and lateral interactions between tubulin dimers, we developed a FRET-based assay that monitors the self-assembly events preceding nucleation (Fig. 2a). When experiments were conducted in the presence of GTP but below the critical concentration for microtubule self-assembly, no microtubules were observed (Supplementary Fig. 2c) yet FRET between tubulin dimers was readily detected, indicative of self-assembly without overt polymerization (Fig. 2b). This assay reports on relevant interactions between tubulin dimers as self-assembly was undetectable in the presence of GDP (Fig. 2f and Supplementary Fig. 2d). Consistent with the finding that deacetylation accelerates a step that precedes nucleation, the pre-nucleation self-assembly rate of deacetylated tubulin was six times faster than that of acetylated tubulin (Fig. 2b,f). Even in the presence of taxol, a strong promoter of microtubule nucleation, self-assembly of tubulin was accelerated four times by deacetylation (Fig. 2c,f). Furthermore, deacetylated tubulin still self-assembled faster than acetylated tubulin in presence of the slowly hydrolysable GTP analogues GTP γ S or GMPCPP (Fig. 2d-f), indicating that acetylation does not exert its effects through a modulation of GTP hydrolysis. Congruently, the rate of GTP hydrolysis during microtubule polymerization was unaffected by the degree of α K40 acetylation (Supplementary Fig. 2e). In this context, it is notable that the catastrophe frequency was unaffected by acetylation, indicating that the stochastic loss of the GTP cap is not influenced by acetylation (Supplementary Fig. 2b).

To determine whether acetylation alters the geometry and strength of longitudinal interactions between tubulin dimers, we assessed protofilament curvature and length after protofilament assembly at 4°C¹⁷ (Fig. 2g and Supplementary Fig. 2f). In agreement with structural studies of α - β end-to-end contacts^{18,19}, GTP γ S, GTP, GMPCPP and GTP/taxol protofilaments became progressively straighter in individually assembled protofilaments (Fig. 2h,i and Supplementary Fig. 3a-f). Importantly, no significant differences in length or radius were detected between deacetylated and acetylated protofilaments regardless of the nucleotide status of tubulin (Fig. 2h,i and Supplementary Fig. 3e,f). Collectively, our analysis of protofilament shape suggests that α K40 acetylation does not modify longitudinal interactions and leaves inter-protofilament interactions as the most likely affected parameter in self-assembly. We note that protofilaments are longer in the presence of GTP γ S (Supplementary Fig. 3e), and the resulting increase in the number of laterally interacting subunits may partially mask the inhibition of self-assembly by acetylation (Fig. 2d,f).

Meanwhile, by straightening protofilaments (Fig. 2i, Supplementary Fig. 3c and Ref. 17,20), taxol facilitates interprotofilament interactions and mitigates the effect of acetylation on self-assembly (Fig. 2c,f). The acetylation-dependent decrease of self-assembly rates is most greatly attenuated by GMPCPP (Fig. 2e,f), likely because GMPCPP both lengthens and straightens protofilaments (Supplementary Fig. 3d-f) thus combining the apparent effects of taxol and GTP γ S on self-assembly.

To directly test the hypothesis that α K40 acetylation weakens lateral interactions, we developed a biophysical FRET-based assay that reports on the strength of inter-protofilament interactions (Fig. 3a). Following the observation that tubulin assembles into protofilaments in the presence of taxol and GTP at 4°C (Supplementary Fig. 3c and Ref. 21) and that at least 85% of the tubulin oligomerizes into protofilaments under these conditions (Supplementary Fig. 3g), we generated labelled protofilaments preparations in GDP-containing buffer (Supplementary Fig. 3h,i). In the absence of GTP, raising the temperature did not lead to microtubule polymerization (see Fig. 4a,b). However, incubation of the protofilaments in the presence of GDP at 32°C led to an increase in FRET signal indicative of protofilament-protofilament interactions (Fig. 3b,e). Because free tubulin incubated under the same conditions did not produce detectable FRET signal (Fig. 3c,e) and free tubulin mixed with protofilaments only yielded a modest FRET signal (Fig. 3d,e), we conclude that longitudinal interactions do not significantly contribute to the FRET signal and that the FRET assay reports on inter-protofilament interactions without signal contamination from the free tubulin remaining in the protofilament preparation. Strikingly, acetylation decreased protofilament self-association five-fold (Fig. 3b,e). Pelleting assays confirmed that a greater mass of oligomers was generated by assembly of deacetylated protofilaments than with acetylated protofilaments (Fig. 3f and Supplementary Fig. 4b). Since neither protofilament length nor curvature were affected by the acetylation status at α K40 (Supplementary Fig. 3i), these results indicate that tubulin acetylation directly reduces either α - α or β - β lateral contacts.

Extending the results from the FRET assay, negative stain EM showed that deacetylated protofilaments assembled into large sheets while acetylated protofilaments remained for the most part isolated with only rare instances of two to three protofilaments associating with one another (Fig. 4a-c and Supplementary Fig. 5a,b). Importantly, analysis of diffraction patterns²² demonstrated that the incubation of protofilaments produced sheets organized in parallel arrays, similarly to the organization of the microtubule lattice (Fig. 4d,e). The diffraction pattern of sheets produced by the protofilament assay was asymmetrical, as was the pattern generated by sheet-like structures at the open ends of microtubules (Fig. 4d,e). Meanwhile the diffraction pattern of antiparallel zinc sheets was instead symmetrical (Fig. 4f). A weakening of lateral α - α or β - β interactions by α K40 acetylation thus provides a unifying explanation for the reduced nucleation rate, accelerated shrinkage and decreased inter-protofilament association of acetylated tubulin (Fig. 1e). Interestingly, while acetylated and deacetylated microtubules assembled from pure tubulin normally have the same number of protofilaments, acetylation enriches 13-protofilament microtubules and depletes 14-protofilament microtubules when microtubules are incubated in the presence of kinesin²³. One interpretation is that, because of slight geometrical differences, lateral interactions in 14-protofilament microtubules are more reliant on α K40 than in 13-protofilament

microtubules. Consequently, acetylation of α K40 may destabilize 14-protofilament microtubules against the torque imposed by the power stroke of kinesin. In agreement with biophysical evidence that lateral contacts between protofilaments are extremely tenuous^{24–26}, a 3.5 Å structure of microtubules finds α - α and β - β contacts consisting of a single aromatic residue captured by a pocket on the lateral neighbor¹⁹. Since α K40 buttresses one of the two loops that form side-to-side contacts²⁷, it has been proposed that an electrostatic bond involving α K40 alters the strength of α - α interactions^{9,23}. This hypothesis has however eluded structural investigations as the nine amino acids flanking α K40 remain the last unsolved part of the α/β -tubulin core¹⁹, even in a 4.2 Å structure of microtubules assembled from non-acetylated recombinant tubulin²⁸. Together, these data suggest that the α K40 loop is flexible and that the lateral contact whose strength is reduced by α K40 acetylation is itself dynamic.

As microtubule acetylation takes place post-assembly in cells and acetylated microtubules are protected from depolymerization³, we rationalized the reduction of inter-protofilament interactions by α K40 acetylation in the biological context of microtubule mechanics. By distributing material away from the central axis, the tubular architecture dramatically increases flexural rigidity compared to a filamentous organization²⁹. At the same time, a longitudinal opening will convert the tube into a highly flexible planar sheet. Similarly, inter-protofilament sliding within the lattice has been proposed to facilitate microtubule bending^{25,30,31}. We predicted that the weakening of lateral interactions by α K40 acetylation may decrease flexural rigidity. Microtubule mechanics were studied using our recently described system³² where dynamic microtubules grow from stabilized microtubule seeds grafted onto micropatterns and are subjected to an orthogonal flow measured *in situ* with fiduciary beads (Fig. 5a). Consistent with our hypothesis, acetylation greatly increased microtubule flexibility (Fig. 5b, Supplementary Fig. 5c,d). Furthermore, similar to microtubules assembled from brain tubulin³², the flexural rigidity of deacetylated microtubules decreased with each consecutive bending cycle, evidencing the material fatigue of deacetylated microtubules (Fig. 5c,d, Supplementary Fig. 5c-f, Supplementary Video 1). In stark contrast, the flexural rigidity of acetylated microtubules remained unchanged in face of repeated bending cycles, thus demonstrating that acetylation suppresses material fatigue and limits the aging of long-lived microtubules.

We propose that the weakening of lateral interactions by α K40 acetylation prevents pre-existing lattice defects from spreading into large areas of damage under repeated stress^{33,34} (Fig. 5e). α K40 acetylation is thus predicted to make long-lived microtubules less susceptible to breakage in contexts where they are subjected to repetitive cycles of bending. The acquisition of microtubule resilience through α K40 acetylation is best exemplified in the touch receptor neurons that run along the longitudinal axis of nematode. The microtubules in these neurons are bent by the sinusoidal movements of the animal and ablation of the α K40 acetyltransferase leads to axonal microtubule breakages^{9,10} that can be rescued by paralyzing the animal¹¹. Cardiomyocytes represent a particularly dramatic example of repeated microtubule stresses as the compressive forces generated by sarcomere shortening are resisted by microtubules that buckle under axial load³⁵. Tubulin detyrosination was found to be important in anchoring stable microtubules to the sarcomere³⁵ and, while there is no direct link between detyrosination and acetylation of

tubulin, it will be of interest to test whether acetylation protects cardiomyocyte microtubules from breakage resulting from repetitive buckling.

Finally, recent studies have found that TAT1 can enter the microtubule either through the ends or through defects along the lattice^{36–38}. Furthermore, it is conceivable that bending produces transient and local breathing events that enable TAT1 entry and local α K40 acetylation³⁷. Local acetylation near lattice defects and areas subjected to stress may therefore increase resilience in areas most prone to mechanical breakage.

Supplementary Material

Refer to Web version on PubMed Central for supplementary material.

Acknowledgements

This work was supported by HFSP Grant RGY0088/2012 to M.V.N. and M.T., ERC grant 310472 to M.T. and a Stanford School of Medicine Dean's Postdoctoral Fellowship to D.P. We thank B.K. Kobilka for the use of his fluorimeter, J. Al-Bassam for advice and assistance on imaging of microtubule dynamics, E. Nogales for comments on the manuscript and E. Verdin for the SIRT2 expression construct. The Jeol JEM1400 TEM was funded by NIH grant 1S10RR02678001 to the Stanford Microscopy Facility.

References

1. Janke C, Bulinski JC. Post-translational regulation of the microtubule cytoskeleton: mechanisms and functions. *Nat Rev Mol Cell Biol.* 2011; 12:773–786. [PubMed: 22086369]
2. Palazzo A, Ackerman B, Gundersen GG. Cell biology: Tubulin acetylation and cell motility. *Nature.* 2003; 421:230. [PubMed: 12529632]
3. Garnham CP, Roll-Mecak A. The chemical complexity of cellular microtubules: tubulin post-translational modification enzymes and their roles in tuning microtubule functions. *Cytoskeleton.* 2012; 69:442–463. [PubMed: 22422711]
4. Soppina V, Herbstman JF, Skiniotis G, Verhey KJ. Luminal localization of α -tubulin K40 acetylation by cryo-EM analysis of fab-labeled microtubules. *PLoS ONE.* 2012; 7:e48204. [PubMed: 23110214]
5. Gittes F, Mickey B, Nettleton J, Howard J. Flexural rigidity of microtubules and actin filaments measured from thermal fluctuations in shape. *J Cell Biol.* 1993; 120:923–934. [PubMed: 8432732]
6. Hawkins T, Mirigian M, Selcuk Yasar M, Ross JL. Mechanics of microtubules. *J Biomech.* 2010; 43:23–30. [PubMed: 19815217]
7. Brangwynne CP, et al. Microtubules can bear enhanced compressive loads in living cells because of lateral reinforcement. *J Cell Biol.* 2006; 173:733–741. [PubMed: 16754957]
8. Bicek AD, et al. Anterograde microtubule transport drives microtubule bending in LLC-PK1 epithelial cells. *Mol Biol Cell.* 2009; 20:2943–2953. [PubMed: 19403700]
9. Cueva JG, Hsin J, Huang KC, Goodman MB. Posttranslational acetylation of α -tubulin constrains protofilament number in native microtubules. *Curr Biol.* 2012; 22:1066–1074. [PubMed: 22658592]
10. Topalidou I, et al. Genetically separable functions of the MEC-17 tubulin acetyltransferase affect microtubule organization. *Curr Biol.* 2012; 22:1057–1065. [PubMed: 22658602]
11. Neumann B, Hilliard MA. Loss of MEC-17 leads to microtubule instability and axonal degeneration. *Cell Rep.* 2014; 6:93–103. [PubMed: 24373971]
12. LeDizet M, Piperno G. Identification of an acetylation site of *Chlamydomonas* alpha-tubulin. *Proc Natl Acad Sci USA.* 1987; 84:5720–5724. [PubMed: 2441392]
13. Voter WA, Erickson HP. The kinetics of microtubule assembly. Evidence for a two-stage nucleation mechanism. *J Biol Chem.* 1984; 259:10430–10438. [PubMed: 6469971]
14. Mandelkow EM, Mandelkow E, Milligan RA. Microtubule dynamics and microtubule caps: a time-resolved cryo-electron microscopy study. *J Cell Biol.* 1991; 114:977–991. [PubMed: 1874792]

15. Molodtsov MI, et al. A molecular-mechanical model of the microtubule. *Biophys J.* 2005; 88:3167–3179. [PubMed: 15722432]
16. VanBuren V, Odde DJ, Cassimeris L. Estimates of lateral and longitudinal bond energies within the microtubule lattice. *Proc Natl Acad Sci USA.* 2002; 99:6035–6040. [PubMed: 11983898]
17. Elie-Caille C, et al. Straight GDP-tubulin protofilaments form in the presence of taxol. *Curr Biol.* 2007; 17:1765–1770. [PubMed: 17919908]
18. Alushin GM, et al. High-resolution microtubule structures reveal the structural transitions in $\alpha\beta$ -tubulin upon GTP hydrolysis. *Cell.* 2014; 157:1117–1129. [PubMed: 24855948]
19. Zhang R, Alushin GM, Brown A, Nogales E. Mechanistic Origin of Microtubule Dynamic Instability and Its Modulation by EB Proteins. *Cell.* 2015; 162:849–859. [PubMed: 26234155]
20. Wang H-W, Long S, Finley KR, Nogales E. Assembly of GMPCPP-bound tubulin into helical ribbons and tubes and effect of colchicine. *Cell Cycle.* 2005; 4:1157–1160. [PubMed: 16123589]
21. Schiff PB, Fant J, Horwitz SB. Promotion of microtubule assembly in vitro by taxol. *Nature.* 1979; 277:665–667. [PubMed: 423966]
22. Shibata K, et al. A single protofilament is sufficient to support unidirectional walking of dynein and kinesin. *PLoS ONE.* 2012; 7:e42990. [PubMed: 22900078]
23. Howes SC, et al. Effects of tubulin acetylation and tubulin acetyltransferase binding on microtubule structure. *Mol Biol Cell.* 2014; 25:257–266. [PubMed: 24227885]
24. Tuszynski JA, Luchko T, Portet S, Dixon JM. Anisotropic elastic properties of microtubules. *Eur Phys J E Soft Matter.* 2005; 17:29–35. [PubMed: 15864724]
25. Pampaloni F, et al. Thermal fluctuations of grafted microtubules provide evidence of a length-dependent persistence length. *Proc Natl Acad Sci USA.* 2006; 103:10248–10253. [PubMed: 16801537]
26. Wu Z, Nogales E, Xing J. Comparative studies of microtubule mechanics with two competing models suggest functional roles of alternative tubulin lateral interactions. *Biophys J.* 2012; 102:2687–2696. [PubMed: 22735518]
27. Nogales E, Whittaker M, Milligan RA, Downing KH. High-resolution model of the microtubule. *Cell.* 1999; 96:79–88. [PubMed: 9989499]
28. Vemu A, et al. Structure and Dynamics of Single-isoform Recombinant Neuronal Human Tubulin. *Journal of Biological Chemistry.* 2016; 291:12907–12915. [PubMed: 27129203]
29. Howard, J. *Mechanics of Motor Proteins and the Cytoskeleton.* Sinauer Associates Incorporated; 2001.
30. Needleman DJ, et al. Radial compression of microtubules and the mechanism of action of taxol and associated proteins. *Biophys J.* 2005; 89:3410–3423. [PubMed: 16100275]
31. Sui H, Sui H, Downing KH, Downing KH. Structural basis of interprotofilament interaction and lateral deformation of microtubules. *Structure.* 2010; 18:1022–1031. [PubMed: 20696402]
32. Schaedel L, et al. Microtubules self-repair in response to mechanical stress. *Nat Mater.* 2015; 14:1156–1163. [PubMed: 26343914]
33. Chrétien D, Metoz F, Verde F, Karsenti E, Wade RH. Lattice defects in microtubules: protofilament numbers vary within individual microtubules. *J Cell Biol.* 1992; 117:1031–1040. [PubMed: 1577866]
34. Schaap IAT, de Pablo PJ, Schmidt CF. Resolving the molecular structure of microtubules under physiological conditions with scanning force microscopy. *Eur Biophys J.* 2004; 33:462–467. [PubMed: 14762705]
35. Robison P, et al. Detyrosinated microtubules buckle and bear load in contracting cardiomyocytes. *Science.* 2016; 352:aaf0659–aaf0659. [PubMed: 27102488]
36. Szyk A, et al. Molecular basis for age-dependent microtubule acetylation by tubulin acetyltransferase. *Cell.* 2014; 157:1405–1415. [PubMed: 24906155]
37. Coombes C, et al. Mechanism of microtubule lumen entry for the α -tubulin acetyltransferase enzyme α TAT1. *Proc Natl Acad Sci U S A.* 2016; doi: 10.1073/pnas.1605397113
38. Ly N, et al. α TAT1 controls longitudinal spreading of acetylation marks from open microtubules extremities. *Sci Rep.* 2016; 6:35624. [PubMed: 27752143]

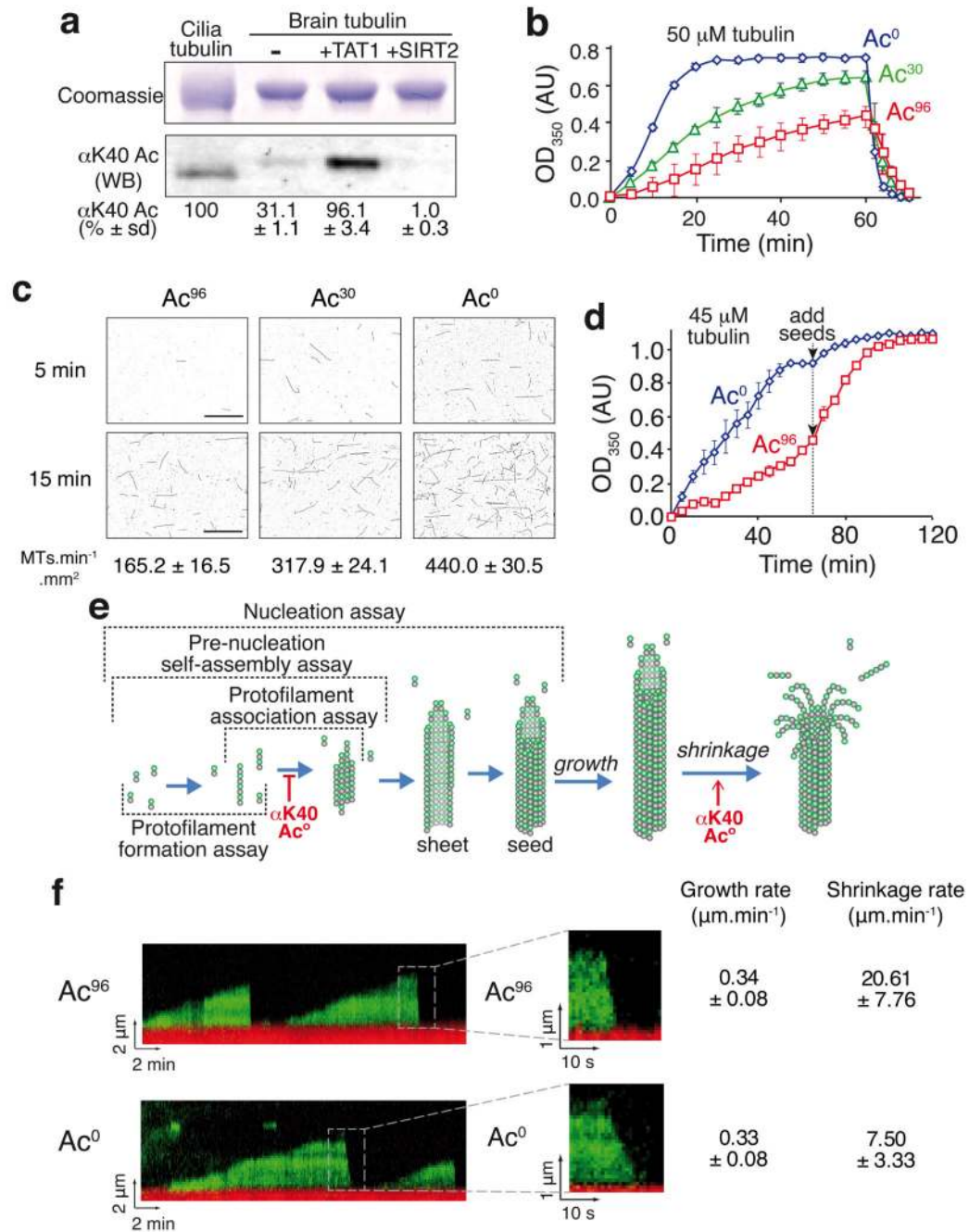


Figure 1. α K40 acetylation impairs microtubule nucleation and accelerates depolymerization.
a. Acetylated (Ac⁹⁶) and deacetylated (Ac⁰) tubulin preparations were produced by treating purified brain tubulin (Ac³⁰) with the acetyltransferase TAT1 or the tubulin deacetylase SIRT2 as detailed in Supplementary Fig. 1a. Samples were resolved on SDS-PAGE and Coomassie-stained (top) or immunoblotted for α K40 acetylation (bottom). Axonemal preparations from *Tetrahymena* cilia provide a 100% acetylation calibrator. The measured levels of α K40 acetylation are shown below (mean of n=3 tubulin preparations \pm SD). Unprocessed original scans of blots are shown in Supplementary Fig. 1c. **b.** Polymer

formation was monitored by following the turbidity, or absorbance at 350 nm, of solutions containing 50 μM tubulin incubated at 37°C. Error bars represent the standard errors of the mean (SEM), $n=3$ independent experiments for Ac^0 , Ac^{30} and Ac^{96} tubulin. **c**, Fluorescence images of microtubules nucleated from 10 μM tubulin solutions incubated at 37°C and fixed at 5 and 15 min (images are representative of 3 independent experiments). The mean rate of microtubule nucleation (\pm SEM) from $n=3$ independent experiments is shown below each image. Scale bar: 10 μm . **d**, Polymer formation was monitored as in **b**, except that starting tubulin concentration was 45 μM and that 5 μM GMPCPP-stabilized microtubule seeds were added after 70 min. Error bars: SEM, $n=3$ independent experiments. **e**, Diagram outlining microtubule nucleation and dynamics. The various assays used in this study are outlined and the effects of tubulin acetylation discovered in this study are shown. **f**, Kymographs of dynamic Ac^{96} and Ac^0 microtubules imaged by TIRF microscopy (representative of 3 independent experiments). In red are the GMPCPP stabilized microtubule seeds and in green the dynamic microtubules elongating from the seed. Insets show depolymerizing microtubules at higher magnification. The rates of growth and shrinkage are shown on the right, $n = 117$ Ac^{96} microtubules and $n = 156$ Ac^0 microtubules (pooled from $n=3$ independent experiments, data are mean \pm SD). Source data for 1b and 1d can be found in Supplementary Table 1.

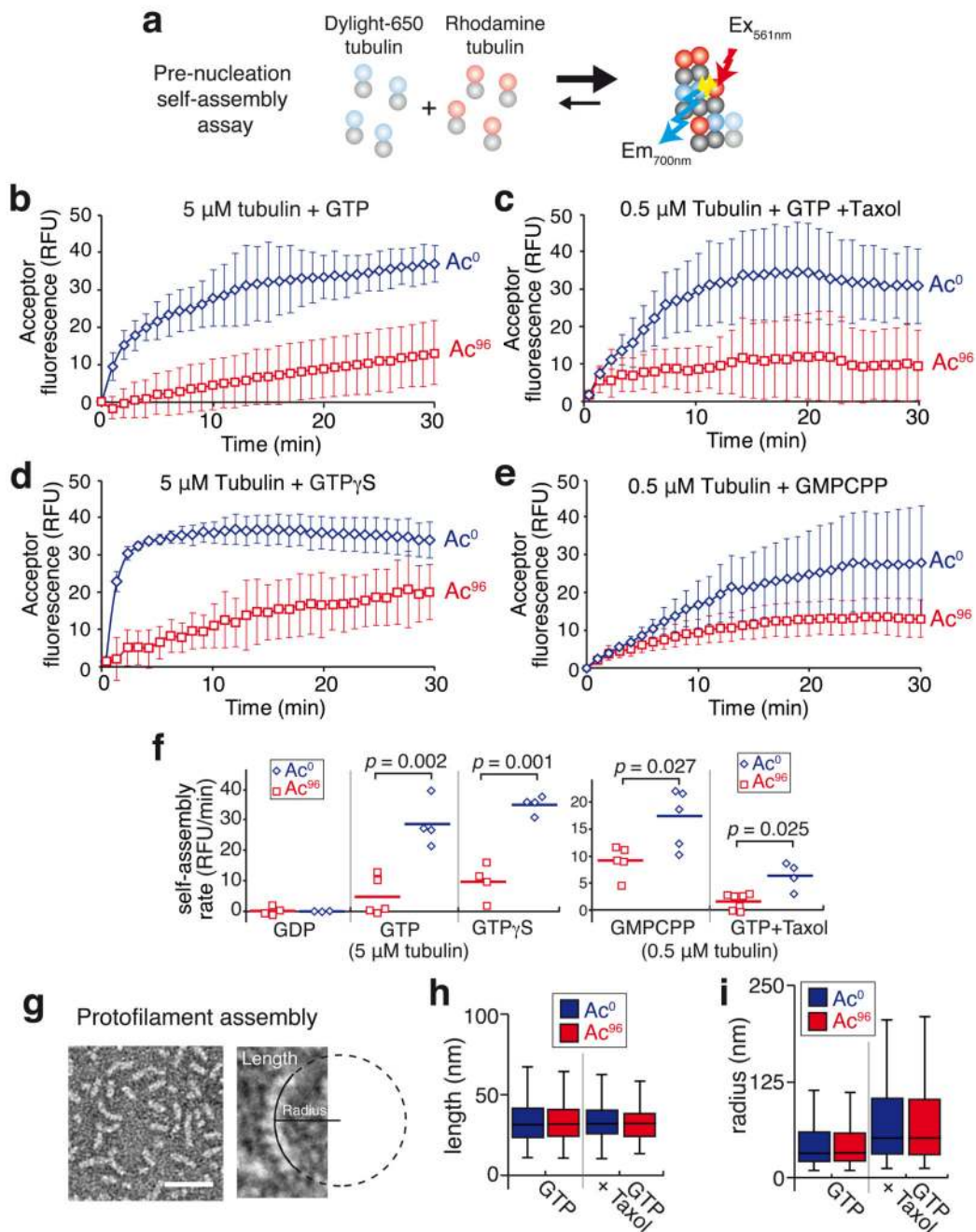


Figure 2. Tubulin acetylation affects tubulin self-assembly

a, Diagram of the FRET-based pre-nucleation self-assembly assay. **b-e**, Tubulin self-assembly assayed by inter-dimer FRET. A solution of free tubulin below the critical concentration for nucleation in which 10% bears a DyLight 650 label and 10% a rhodamine-label was incubated at 37°C and self-assembly was followed in a spectrofluorimeter by exciting rhodamine at 561 nm and measuring DyLight 650 emission at 700 nm. Data points are mean \pm SEM, **b**, 5 μM tubulin was mixed with 1 mM GTP. $n=5$ for Ac^{96} and $n=4$ for Ac^0 tubulin. **c**, 0.5 μM tubulin was mixed with 1 mM GTP + 0.5 μM taxol. $n=7$ for Ac^{96} and

n=4 for Ac⁰ tubulin. **d**, 5 μM tubulin was mixed with 1 mM GTPγS. n=4 for both Ac⁹⁶ and Ac⁰ tubulin. **e**, 0.5 μM tubulin was mixed with 0.5 mM GMPCPP. n=5 for both Ac⁹⁶ and Ac⁰ tubulin. n values represent the number of independent experiments. **f**, Dot plot of the pre-nucleation self-assembly rates for Ac⁹⁶ and Ac⁰ tubulin. The experiment was done using 5 μM of free tubulin with 1 mM GDP, 1 mM GTP or 1 mM GTPγS, or 0.5 μM of free tubulin with 1 mM GTP + 0.5 μM taxol or 0.5 mM GMPCPP. The bar denotes the mean. The *p*-values were calculated using a two-tailed unpaired Student's *t*-test. **g**, Taxol-stabilized protofilaments observed by negative stain electron microscopy. The length of each protofilament was measured and a circle was fitted onto the protofilament to measure the radius (images representative of 2 independent experiments). **h,i**, Box plots of the length (**h**) and radius (**i**) of the Ac⁰ (blue boxes) and Ac⁹⁶ (red boxes) protofilaments assembled in the presence of GTP or GTP+taxol. For the GTP condition: n=612 Ac⁰ protofilaments and n=513 Ac⁹⁶ protofilaments, for the GTP+taxol condition: n=542 Ac⁰ protofilaments and n=536 Ac⁹⁶ protofilaments (pooled from 2 independent experiments). A Mann-Whitney test was used to compare Ac⁰ and Ac⁹⁶ protofilaments populations in each condition. No significant differences were observed between Ac⁰ and Ac⁹⁶ protofilaments in length (*p*=0.74 for GTP and *p*=0.07 for GTP+taxol) or radius (*p*=0.64 for GTP and *p*=0.94 for GTP+taxol). The box represents the 25th-75th percentile, whiskers indicate 1.5 times the range and the bar in the middle is the median.

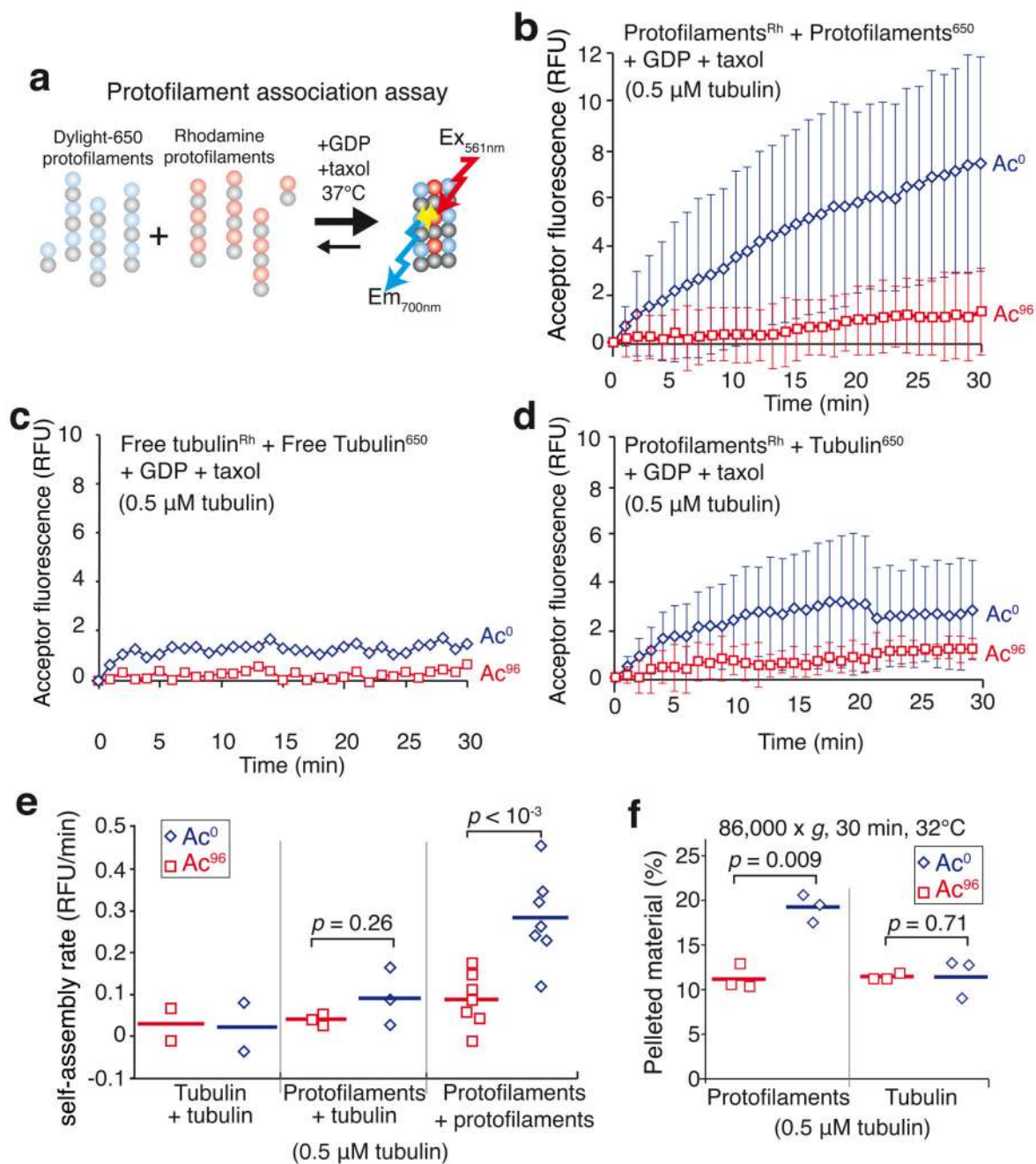


Figure 3. αK40 acetylations

a, Diagram of the FRET-based protofilament association assay. Two populations of taxol-stabilized protofilaments were mixed together in the presence of taxol and GDP at 37°C and self-association was followed by monitoring the fluorescence transferred between protofilaments. **b-d**, Self-assembly was assayed in the presence of 1 mM GDP and 0.5 μM taxol at 32°C. FRET was followed in a spectrofluorimeter by exciting rhodamine at 561 nm and measuring DyLight 650 emission at 700 nm. **(b)** Rhodamine-labeled protofilaments were mixed with DyLight 650-labeled protofilaments (each made with a molar ratio of 90%

unlabeled tubulin to 10% labeled tubulin). Data points are mean \pm SEM. $n = 7$ independent experiments for both Ac⁹⁶ and Ac⁰ tubulin. (c) Rhodamine- and DyLight 650-labeled tubulin stocks were mixed with unlabeled tubulin so that 10% of the tubulin was rhodamine-labeled and 10% DyLight 650-labeled. Data points are mean of $n = 2$ experiments for both Ac⁹⁶ and Ac⁰ tubulin. (d) Protofilaments (molar ratio of 90% unlabeled tubulin to 10% rhodamine-labeled tubulin) were mixed with free tubulin (molar ratio of 95% unlabeled tubulin to 5% DyLight 650-labeled tubulin) to mimic the free tubulin left in solution after protofilament assembly. Data points are mean \pm SEM. $n = 3$ independent experiments for both Ac⁹⁶ and Ac⁰ tubulin. e, Dot plot of the self-assembly rates for free tubulin, free tubulin with protofilaments or protofilaments incubated in the presence of 1 mM GDP and 0.5 μ M taxol at 32°C. The bar denotes the mean. Total tubulin concentration was 0.5 μ M. The p -values of the two-tailed unpaired Student's t -tests are indicated. f, Dot plot of the amount of tubulin pelleted at $86,000 \times g_{ave}$ for 30 min at 32°C as a result of the association amongst Ac⁰ or Ac⁹⁶ protofilaments ($n=3$ independent experiments). The bar denotes the mean. The p -values of the two-tailed unpaired Student's t -tests are indicated. Source data for 3c and 3d can be found in Supplementary Table 1.

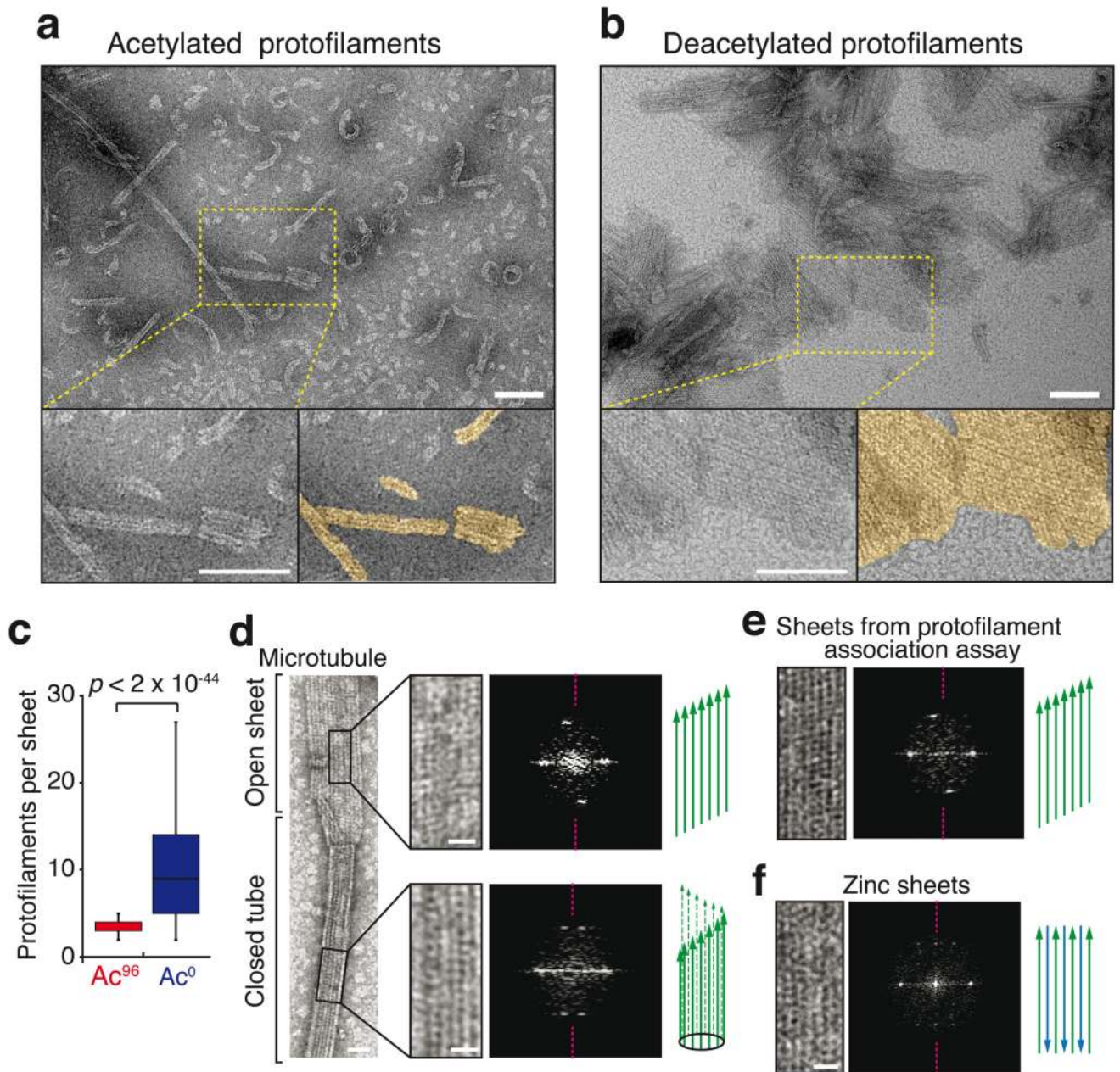


Figure 4. The protofilament interaction assay produces parallel sheets.

a,b, EM micrographs of the protofilaments interaction assays (images are representative of 2 independent experiments). Protofilaments were incubated at 32°C for 30 min with 0.5 μ M taxol and 1 mM GDP, and imaged by negative-stain EM. The few sheets observed with Ac^{96} protofilaments contained only 2 to 5 protofilaments (**a**), while extended sheets are seen with Ac^0 protofilaments (**b**). Scale bar = 100 nm. Protofilaments sheets are highlighted in gold color in the magnified bottom right panel of (**a**) and (**b**). Scale bar: 100 nm. **c**, Box plots of the width of sheets (expressed in contiguous protofilament numbers) formed by the association of Ac^0 or Ac^{96} protofilaments. $n = 361$ Ac^{96} protofilaments and $n = 382$ Ac^0

protofilaments (pooled from 2 independent experiments). The box represents the 25th-75th percentile, whiskers indicate 1.5 times the range, bar in the middle is the median **d-f**, Negative stain EM images and associated diffraction patterns; magenta dashed lines indicate the meridian of the diffraction pattern. **d**, The closed microtubule lattice and its diffraction pattern is shown in the bottom right panels while the open sheet and its diffraction patterns is shown on the top right panels. **e**, Protofilament sheet and its diffraction patterns from the protofilament self-assembly assay. **f**, Antiparallel protofilament sheet assembled in presence of zinc. Scale bars: 25 nm (full size images), 10 nm (magnified insets). Diagrams illustrate the known and deduced protofilaments organization. The experiments presented in **d** and **f** were performed once, and the experiment in **e** twice.

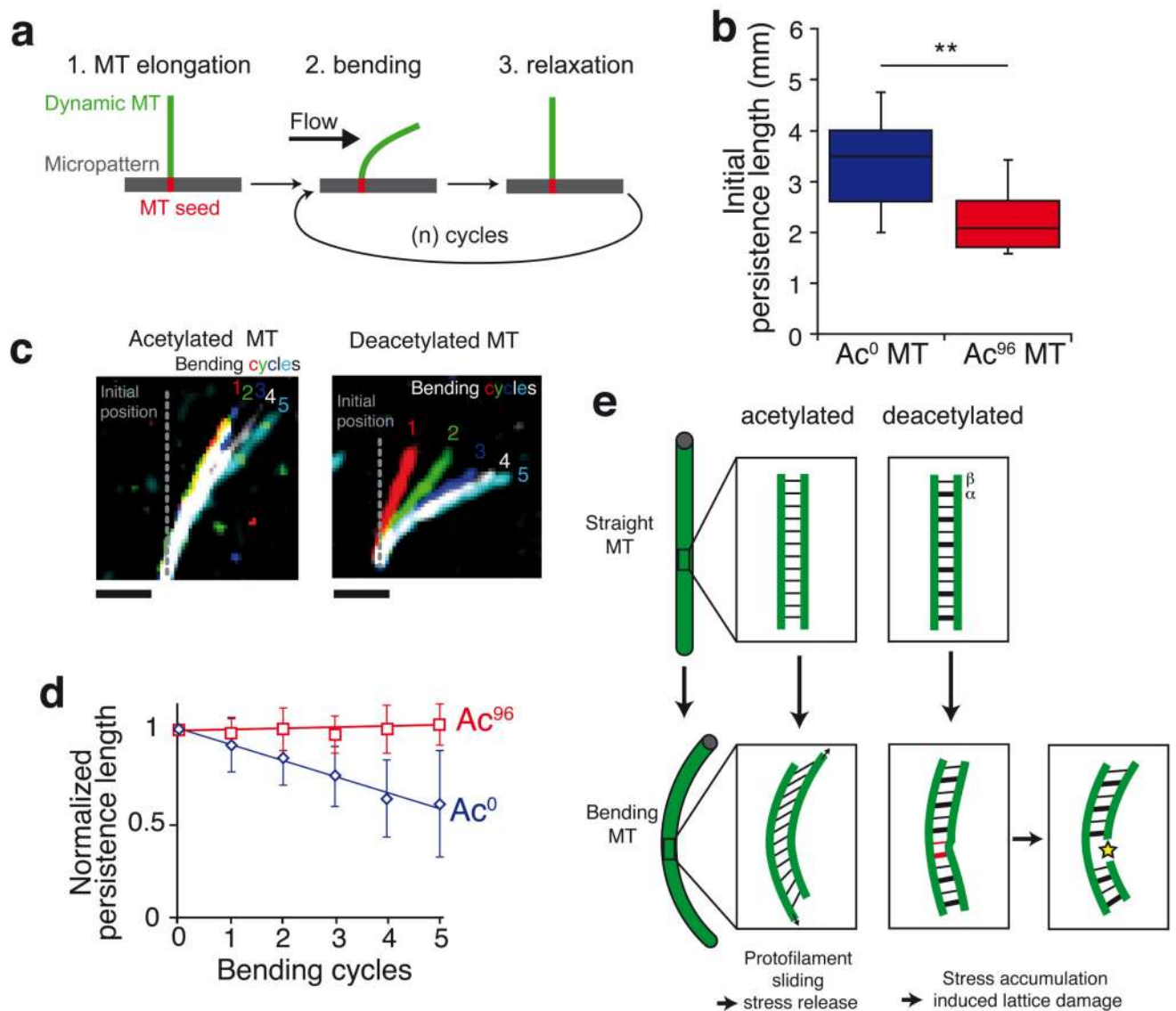


Figure 5. Acetylation at α K40 protects microtubules against stress-induced material fatigue.

a, Diagram representing the experimental setup used to measure microtubule flexibility and material fatigue. Microtubules were elongated from GMPCPP seeds grafted onto micropatterns, bent using a perpendicular flow for 10 s and then allowed to relax for 10 s. The microtubules are kept dynamic during the experiment by maintaining tubulin concentration at 14 μ M in the flowing solution. **b**, Microtubule persistence lengths measured during the first bending cycle. ** denotes a p -value of the two-tailed unpaired Student's t -test < 0.01 , $n = 11$ Ac⁹⁶ microtubules and $n = 17$ Ac⁰ microtubules. The box represents the 25th-75th percentile, whiskers indicate 1.5 times the range, bar in the middle is the median. **c**, Pseudocolor images of a single representative microtubule at the end of each bending cycle. Scale bar = 5 μ m. **d**, Plot showing the evolution of persistence length over successive bending cycles. Microtubule persistence lengths were normalized to their initial values (the non-normalized data are shown in Supplementary Figure 5c and d). Data points are mean \pm SD, n

= 11 Ac⁹⁶ microtubules and n= 17 Ac⁰ microtubules. **e**, Model accounting for the increased flexibility and mechanical stability of acetylated microtubules due to decreased interprotofilament interactions.